Min-Max Hamming Distance Considerations for Activation Pattern Design in Index Modulation

Yinglin Chen
6G Research Center
China Telecom Research Institute
Guangzhou, China
chenyl37@chinatelecom.cn

Tongyang Xu
Dept. Electronic and Electrical Engineering
University College London
London, United Kingdom
tongyang.xu.11@ucl.ac.uk

Izzat Darwazeh
Dept. Electronic and Electrical Engineering
University College London
London, United Kingdom
i.darwazeh@ucl.ac.uk

***Abstract*—Index modulation (IM) has been widely studied showing promising performance over traditional communication systems. Index pattern plays an important role since its activation methodology determines bit error rate (BER), spectral efficiency (SE) and energy efficiency (EE). This work proposes efficient index activation patterns according to a min-max Hamming distance metric for both orthogonal frequency division multiplexing (OFDM) and non-orthogonal spectrally efficient FDM (SEFDM). Simulations of low-density parity-check (LDPC) coded IM systems in both additive white Gaussian noise (AWGN) and frequency selective channels are provided. Results reveal that the proposed index activation patterns in IM systems lead to improved BER and SE compared to that in traditional OFDM systems. Moreover, peak-to-average power ratio (PAPR) distribution results are presented to demonstrate the EE advantage of the proposed IM systems over OFDM systems.**

***Index Terms*—Index modulation, OFDM, SEFDM, activation pattern, Hamming distance, PAPR**

I. Introduction

Index modulation (IM) with high spectral efficiency and high energy efficiency is considered as a promising next-generation transmission technology [1]. The basic concept of IM is to embed implicit information bits on the states of certain communication resource entities (e.g. antennas, subcarriers, time slots) along with the information bits explicitly transmitted by conventional digital modulation schemes. IM was originally introduced by spatial modulation (SM), where index information is conveyed by the activation states of antennas in a multiple-input multiple-output (MIMO) system [2]. Inspired by the spatial-domain modulation, IM was integrated in multicarrier systems in [3]. The IM principle can also be applied in time domain [4], in which data transmission is manipulated on different time slots. Apart from the aforementioned single-domain IM schemes, multi-dimensional IM schemes were proposed to further enhance the system flexibility by combining various single-domain IM options. A comprehensive overview of up-to-date IM schemes can be found in [5], [6].

Substantial research was conducted on combining the IM principle with orthogonal frequency division multiplexing (OFDM), which is a broadly used waveform in modern communications. To address the error propagation problem in the early work [3], subcarrier grouping was proposed in OFDM with IM (OFDM-IM), which divides subcarriers into subblocks and performs subblock-based index modulation and demodulation to reduce computational complexity [7]. In OFDM-IM, only a part of subcarriers are activated and additional information is conveyed by their indices without energy consumption. By allocating the saved transmission power to the activated subcarriers, OFDM-IM obtains error performance improvement compared to OFDM. Moreover, the deactivated subcarriers can reduce peak-to-average power ratio (PAPR) of OFDM and bring increased energy efficiency [8]. To compensate for the spectral efficiency loss due to the deactivated subcarriers, a variety of index designs were proposed based on OFDM-IM. On one hand, the achievable spectral efficiency of OFDM-IM can be enhanced by flexible IM patterns such as dual-mode IM (DM) [9] where all subcarriers are activated and modulated with two distinguishable modulation schemes. On the other hand, spectral efficiency can be increased by replacing OFDM with spectrally efficient FDM (SEFDM). SEFDM achieves increased spectral efficiency by placing subcarriers at a frequency spacing smaller than the symbol rate [10]. In this case, SEFDM with IM (SEFDM-IM) [11] not only achieves higher spectral efficiency from non-orthogonal waveform utilization and rich index variants, but also efficiently mitigates inter-carrier interference (ICI) because of the deactivated subcarriers. A Gray-coded strategy for the mapping between index bits and antenna activation order was proposed for differential SM (DSM) with improved error performance reported [12]. It was also adopted in DM to design constellation mapping [13]. However, the strategy does not allow for a quantified comparison of activation pattern designs. In addition, previous work was limited to OFDM waveform without considering other waveform candidates.

In this work, we define two parameters namely Hamming distance for similarity and Hamming distance for difference to enable analytical comparisons of possible activation pattern designs and propose a design principle accordingly. In addition, we examine the activation pattern design principle on OFDM-IM and SEFDM-IM systems in a low-density parity-check (LDPC) coded scenario. By simulation results, we verify that the proposed design principle achieves improved bit error rate (BER) performance, which is robust to ICI impairment and frequency selective fading.

The rest of the paper is organized as follows. Section II

provides the coded SEFDM-IM system model, and Section III presents the activation pattern design principle. Simulation results in Section IV verify the superiority of the proposed principle and conclusions are drawn in Section V.

II. System Model

A. Transmitter Design

As seen from Fig. 1, an information bit stream $\mathcal{B}$ of length B is encoded into a B_c-length bit stream for an SEFDM-IM symbol transmission, and the coding rate is $\mathcal{R} = B/B_c$. The coded bit stream $\mathcal{C}$ is split into G groups, and each group consists of $L = B_c/G$ bits. The first L_1 index bits enter the activation pattern selector and yield the activation pattern for an SEFDM-IM subblock, which is expressed as

$$I^g = \left\{ i_1^g, i_2^g, \cdots, i_{N_S}^g \right\}, \tag{1}$$

for $1 \leq g \leq G$. $i_\chi^g \in \{0, 1\}$ for $\chi = 1, 2, ..., N_S$, and N_S denotes the number of subcarriers in each subblock. The χ-th subcarrier in the g-th subblock is activated when $i_\chi^g = 1$, and it is deactivated when $i_\chi^g = 0$. Since N_A out of N_S subcarriers are selected to be activated based on the input index bits, a total of $L_1 = \left\lfloor \log_2 \binom{N_S}{N_A} \right\rfloor$ index bits can be transmitted in one subblock, where $\lfloor \cdot \rfloor$ denotes the floor function. Given $\binom{N_S}{N_A}$ possible activation patterns, we choose 2^{L_1} legal activation patterns out of them based on a proposed principle described in the next section. The set of these legal activation patterns is denoted as $\mathcal{I}$.

The remaining $L_2 = L - L_1$ data bits are mapped on to N_A data symbols with the M-ary digital modulation technique. In other words, we have the g-th data symbol vector expressed as

$$P^g = \left[\rho_1^g, \rho_2^g, \cdots, \rho_{N_A}^g \right]^T, \tag{2}$$

where $[\cdot]^T$ is the transpose operator. We have $P^g \in \Lambda^{N_A}$, and Λ is the alphabet of the M-ary signal constellation, which is scaled by $\sqrt{N_S/N_A}$ to maintain unit average power. The output of the g-th symbol mapper is given by

$$S^g = \mathbf{A}^g \cdot P^g, \tag{3}$$

where $\mathbf{A}^g$ is an $N_S \times N_A$ activation matrix whose columns are extracted from an $N_S \times N_S$ identity matrix for those indices associated with the activated subcarriers. As an example, the G-th subblock with $I^G = \{0, 1, 1, 0\}$ is given by

$$S^G = \begin{bmatrix} 0 & 0 \\ 1 & 0 \\ 0 & 1 \\ 0 & 0 \end{bmatrix} \cdot \begin{bmatrix} \rho_1^G \\ \rho_2^G \end{bmatrix} = \left[0, \rho_1^G, \rho_2^G, 0 \right]^T. \tag{4}$$

The SEFDM-IM block is then formed by concatenating G subblocks, given by

$$S = \left[S^1, S^2, \cdots, S^G \right]^T = \left[s_1, s_2, \cdots, s_N \right]^T, \tag{5}$$

where $s_k \in \{0, \Lambda\}$ for $k = 1, 2, ..., N$, and $N = N_S G$ is the system size. SEFDM modulation is represented by

$$X = \mathbf{\Phi} \cdot S, \tag{6}$$

where $X = [x_1, x_2, \cdots, x_N]^T$, and $\mathbf{\Phi}$ is a subcarrier matrix whose elements equal to $\mathbf{\Phi}_{k,n} = (1/\sqrt{N}) e^{j2\pi\alpha \frac{kn}{N}}$ for $n = 1, 2, ..., N$. The bandwidth compression factor α is defined as $\alpha = \Delta f T$, where Δf is the frequency spacing between two adjacent subcarriers and T denotes the SEFDM-IM symbol period. An SEFDM-IM signal has α smaller than 1, and it is converted to an OFDM-IM signal when α is 1. Inverse discrete Fourier transform (IDFT)-based modulation could be deployed [14]. Consequently, the spectral efficiency of the SEFDM-IM system is calculated as

$$\text{SE} = \frac{\mathcal{R} L}{\alpha N_S}. \tag{7}$$

The introduction of the bandwidth compression factor α increases the achievable spectral efficiency.

B. Receiver Design

The received signal contaminated by the AWGN channel is expressed as $Y = X + W$. The AWGN vector $W = [w_1, w_2, \cdots, w_N]^T$ comprises N noise samples that follow a complex Gaussian distribution denoted as $\mathcal{CN}(0, N_0)$, where N_0 denotes the noise variance. SEFDM demodulation is given by

$$R = \mathbf{\Phi}^H \cdot Y = \mathbf{\Phi}^H \cdot \mathbf{\Phi} \cdot S + \mathbf{\Phi}^H \cdot W = \boldsymbol{C} \cdot S + W_{\mathbf{\Phi}^H}, \tag{8}$$

where $[\cdot]^H$ is the Hermitian transpose operator. $W_{\mathbf{\Phi}^H}$ is the demodulated noise term, and $\boldsymbol{C}$ denotes the correlation matrix defined as $\boldsymbol{C} = \mathbf{\Phi}^H \mathbf{\Phi}$. In the case of OFDM-IM, the off-diagonal entries in the correlation matrix $\boldsymbol{C}$ are close to zero because of the orthogonality between subcarriers. For SEFDM-IM signals, the non-zero off-diagonal entries characterise the interference caused by non-orthogonally packed subcarriers.

Concerning the computational complexity, we assume that subblocks can be independently detected and divide the demodulated signal R into G subblocks, each denoted as R^g. After that, the log-likelihood ratio (LLR) values of bits transmitted in each subblock are computed in the LLR calculator for LDPC decoding. We define $\mathcal{I}_{l,0}$ and $\mathcal{I}_{l,1}$ as the subsets of $\mathcal{I}$ that convey a '0' and a '1' at the l-th index place, respectively. In the g-th subblock, the l-th index bit denoted as ${\mathcal{C}_1}^g(l)$ for $l = 1, 2, ..., L_1$ has the LLR value of

$$\lambda\left({\mathcal{C}_1}^g(l) | R^g\right) = \ln \frac{\Pr\left({\mathcal{C}_1}^g(l) = 0 | R^g\right)}{\Pr\left({\mathcal{C}_1}^g(l) = 1 | R^g\right)}, \tag{9}$$

where $\Pr(\cdot)$ is the probability operator. The same a priori probabilities are assumed for all legal activation patterns and data symbols, and therefore (9) is converted to

$$\lambda\left({\mathcal{C}_1}^g(l) | R^g\right) = \ln \frac{\sum\limits_{I^g \in \mathcal{I}_{l,0}} \sum\limits_{P^g \in \Lambda^{N_A}} \Pr\left(R^g | S^g\right)}{\sum\limits_{I^g \in \mathcal{I}_{l,1}} \sum\limits_{P^g \in \Lambda^{N_A}} \Pr\left(R^g | S^g\right)}, \tag{10}$$

where S^g is computed from I^g and P^g according to (3). For convenience of presentation, we define $\Theta\left(I^g, P^g\right)$ as

$$\Theta\left(I^g, P^g\right) = \frac{1}{N_0} \left(R^g - \boldsymbol{C}^g S^g\right)^H \left(R^g - \boldsymbol{C}^g S^g\right), \tag{11}$$

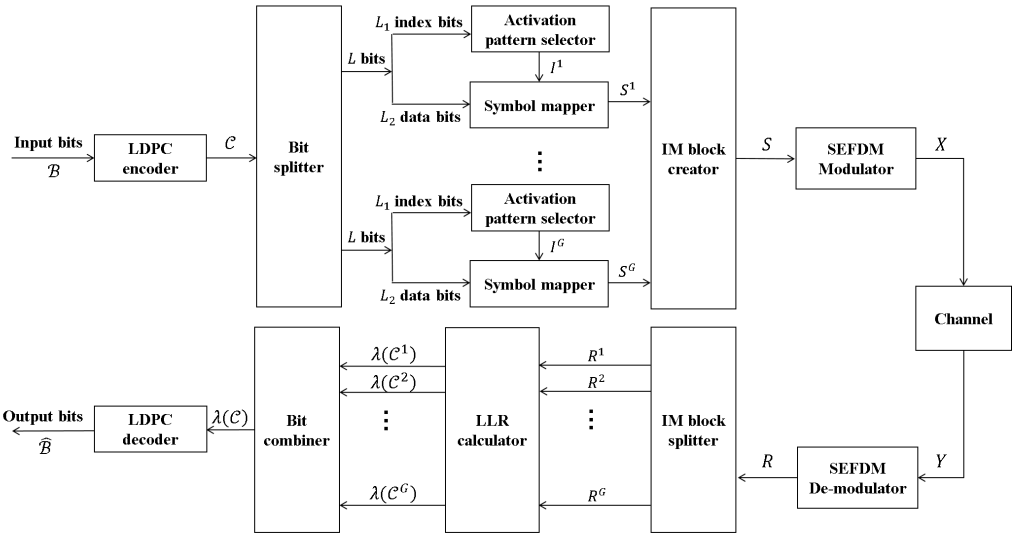

Fig. 1. Block diagram of the LDPC-coded SEFDM-IM transceiver.

where $\boldsymbol{C}^g$ is an $N_S \times N_S$ sub-matrix created by the elements in $\boldsymbol{C}$ whose column and row indices are both within the range of $[(g-1)N_S+1, gN_S]$. Then, the likelihood function $\Pr(R^g|S^g)$ is given by

$$\Pr\left(R^g|S^g\right) = \frac{e^{-\Theta(I^g,P^g)}}{\pi N_0}. \tag{12}$$

The LLR calculation of index bits given in (10) is therefore simplified to

$$\lambda\left({\mathcal{C}_1}^g(l)\,|R^g\right) = \ln \frac{\sum\limits_{I^g\in\mathcal{I}_{l,0}} \sum\limits_{P^g\in\Lambda^{N_A}} e^{-\Theta(I^g,P^g)}}{\sum\limits_{I^g\in\mathcal{I}_{l,1}} \sum\limits_{P^g\in\Lambda^{N_A}} e^{-\Theta(I^g,P^g)}}. \tag{13}$$

Similar LLR calculations are performed on data bits. $\Lambda_{v,0}^{N_A}$ and $\Lambda_{v,1}^{N_A}$ are defined as the subsets of Λ^{N_A} that convey a '0' and a '1' as the v-th data bit for $v = 1, 2, ..., L_2$, respectively. We use ${\mathcal{C}_2}^g(v)$ to denote the v-th data bit in the g-th subblock, and it has the LLR value of

$$\begin{aligned}\lambda\left({\mathcal{C}_2}^g(v)\,|R^g\right) &= \ln \frac{\Pr\left({\mathcal{C}_2}^g(v)=0|R^g\right)}{\Pr\left({\mathcal{C}_2}^g(v)=1|R^g\right)} \\ &= \ln \frac{\sum\limits_{I^g\in\mathcal{I}} \sum\limits_{P^g\in\Lambda_{v,0}^{N_A}} e^{-\Theta(I^g,P^g)}}{\sum\limits_{I^g\in\mathcal{I}} \sum\limits_{P^g\in\Lambda_{v,1}^{N_A}} e^{-\Theta(I^g,P^g)}}.\end{aligned} \tag{14}$$

Notice that no assumption is made on subcarriers' activation states based on the LLR results of index bits. This is to avoid the situation where an erroneous detection of index bits affects the detection of data bits. The exhaustive search gives the optimal LLR calculation.

Next, the LLR values of bits transmitted in the g-th subblock denoted as $\lambda(\mathcal{C}^g)$ are obtained by concatenating $\lambda({\mathcal{C}_1}^g)$ and $\lambda({\mathcal{C}_2}^g)$. The LLR values of bits transmitted in one SEFDM-IM symbol are then converted into one stream denoted as $\lambda(\mathcal{C})$, which is sent into the LDPC decoder to yield the output bit stream $\widehat{\mathcal{B}}$.

TABLE I
THE CONVENTIONAL ACTIVATION PATTERN DESIGN [7].

Pattern	*Index bits*	*Activation pattern*
1	[0, 0]	$\iota_1 = \{1,\ 1,\ 0,\ 0\}$
2	[0, 1]	$\iota_2 = \{0,\ 1,\ 1,\ 0\}$
3	[1, 0]	$\iota_3 = \{0,\ 0,\ 1,\ 1\}$
4	[1, 1]	$\iota_4 = \{1,\ 0,\ 0,\ 1\}$

III. ACTIVATION PATTERN DESIGN

In this section, we demonstrate our design principle and provide two proposed activation pattern designs. The conventional activation pattern design deployed in [7] is shown in Table I. We define Hamming distance for similarity D_S as the average Hamming distance between activation patterns that correspond to the same index bit (i.e. '0' or '1'). As an example in Table I, the average Hamming distance for similarity of the first index bit is given by

$$D_{S,1} = \frac{D_h(\iota_1,\iota_2)+D_h(\iota_3,\iota_4)}{2} = 2, \tag{15}$$

where $D_h(\iota_1,\iota_2)$ finds the Hamming distance between activation patterns ι_1 and ι_2 since they have the same bit (i.e. '0') at the first index place. $D_h(\iota_3,\iota_4)$ indicates the Hamming distance between activation patterns ι_3 and ι_4 because they have the same bit (i.e. '1') at the first index place.

Following the same principle, the average Hamming distance for similarity of the second index bit is given by

$$D_{S,2} = \frac{D_h(\iota_1,\iota_3)+D_h(\iota_2,\iota_4)}{2} = 4. \tag{16}$$

Therefore, the Hamming distance for similarity of the conventional activation pattern design in Table I is given by

$$D_S = \frac{D_{S,1}+D_{S,2}}{2} = 3. \quad (17)$$

We then define Hamming distance for difference D_D as the average Hamming distance between activation patterns that correspond to two different index bits. The Hamming distance for difference of the first index bit in the conventional activation pattern design in Table I is given by

$$D_{D,1} = \frac{D_h(\iota_1,\iota_3)+D_h(\iota_1,\iota_4)+D_h(\iota_2,\iota_3)+D_h(\iota_2,\iota_4)}{4} = 3, \quad (18)$$

where $D_h(\iota_1, \iota_3)$ gives the Hamming distance between activation patterns ι_1 and ι_3 because they have a '0' and a '1' at the first index place, respectively. The same calculation performed on the second index bit is expressed as

$$D_{D,2} = \frac{D_h(\iota_1,\iota_2)+D_h(\iota_1,\iota_4)+D_h(\iota_2,\iota_3)+D_h(\iota_3,\iota_4)}{4} = 2. \quad (19)$$

The Hamming distance for difference of the conventional activation pattern design is therefore

$$D_D = \frac{D_{D,1}+D_{D,2}}{2} = 2.5. \quad (20)$$

To improve the detection probability of index bits, the Hamming distance for similarity should be minimized and the Hamming distance for difference should be maximized. Following the min-max Hamming distance principle, we propose two activation pattern designs denoted as proposed-1 and proposed-2 in Table II. Furthermore, Table III provides their Hamming distance comparisons. The proposed-2 design achieves the lowest D_S value and the highest D_D value. In other words, it is designed to obtain the best min-max Hamming distance metric and expected to give the lowest BER among all possible activation designs.

We use the percentage change in D_S and D_D with respect to the values of the proposed-2 design to compare between the proposed-1 design and the conventional design. As seen from Table III, compared to the proposed-2 design, the proposed-1 design is degraded by 25% in terms of D_S and D_D, while the conventional design is degraded by 50% and 16.7% in terms of D_S and D_D, respectively. Therefore, it is expected that the proposed-1 design also outperforms the conventional design in BER performance. Although this work only discusses activation patterns with $N_S = 4$ and $N_A = 2$, the proposed min-max Hamming distance principle can be applied to other N_S and N_A configurations as well as IM variants such as DM.

IV. Results and Discussions

In this section, we present the error performance of OFDM-IM and SEFDM-IM systems with the proposed-1, proposed-2 and conventional activation pattern designs described above. To provide a comprehensive analysis of system performance, their PAPR distributions are also presented by the complementary cumulative distribution function (CCDF). The performance of the traditional OFDM system is provided as a benchmark. The figure legend specifies the utilized activation pattern design and modulation scheme. IM is mainly designed for low-power communication systems such as narrowband Internet of things (NB-IoT). Therefore, this work considers systems with 12 subcarriers, i.e. $N = 12$.

TABLE II
The Proposed Activation Pattern Designs.

Pattern	*Index bits*	*Proposed-1*	*Proposed-2*
1	[0, 0]	$\iota_1 = \{1,\ 1,\ 0,\ 0\}$	$\iota_1 = \{1,\ 0,\ 0,\ 1\}$
2	[0, 1]	$\iota_2 = \{1,\ 0,\ 1,\ 0\}$	$\iota_2 = \{1,\ 0,\ 1,\ 0\}$
3	[1, 0]	$\iota_3 = \{1,\ 0,\ 0,\ 1\}$	$\iota_3 = \{0,\ 1,\ 0,\ 1\}$
4	[1, 1]	$\iota_4 = \{0,\ 1,\ 0,\ 1\}$	$\iota_4 = \{0,\ 1,\ 1,\ 0\}$

TABLE III
The Hamming Distance for Similarity and The Hamming Distance for Difference of Different Activation Pattern Designs.

Design	D_S	D_D	*% change in* D_S	*% change in* D_D
Proposed-1	2.5	2.25	+25%	-25%
Proposed-2	2	3	-	-
Conventional	3	2.5	+50%	-16.7%

In Fig. 2, 4QAM modulation (i.e. $M = 4$) is deployed in OFDM-IM and SEFDM-IM systems. To obtain the same spectral efficiency of 0.9 bit/s/Hz, OFDM-IM with $\alpha = 1$ and SEFDM-IM with $\alpha = 5/6$ are applied with the LDPC coding rates of $R = 0.6$ and $R = 0.5$, respectively. It is observed that OFDM-IM with the proposed-2 activation pattern design achieves 0.72 dB better performance over the conventional design. The power gain achieved by the proposed-1 OFDM-IM activation pattern is reduced to 0.15 dB when comparing to the conventional OFDM-IM system. The reason is that

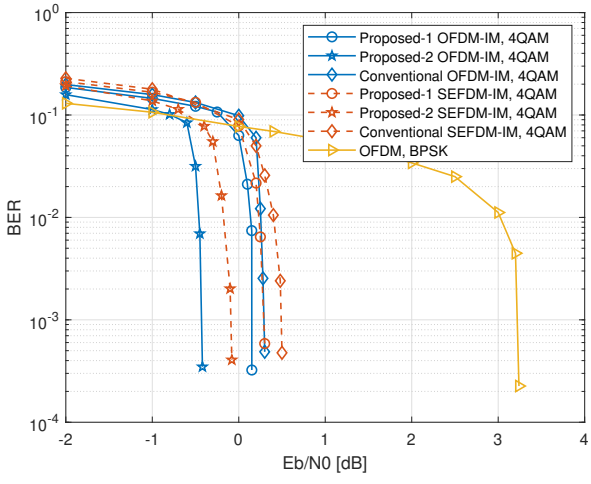

Fig. 2. BER performance of OFDM-IM, SEFDM-IM and OFDM with the spectral efficiency of 0.9 bit/s/Hz in the AWGN channel.

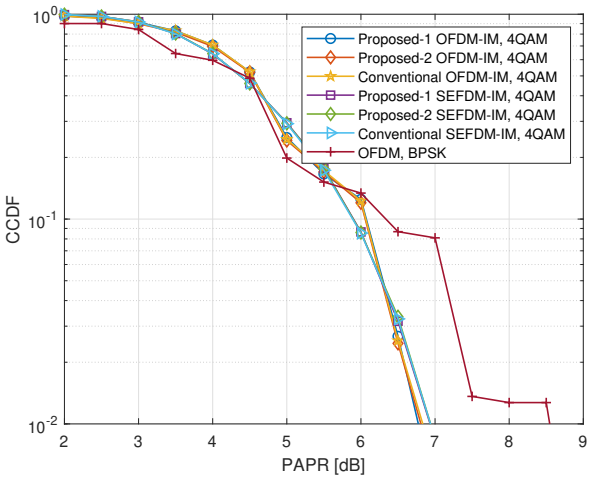

Fig. 3. PAPR distribution of OFDM-IM, SEFDM-IM and OFDM with the spectral efficiency of 0.9 bit/s/Hz.

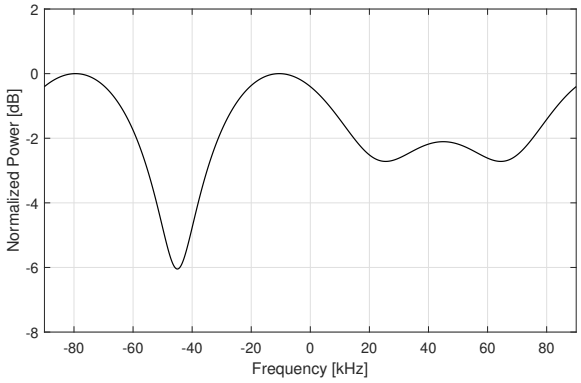

Fig. 4. Channel response for the three-path static frequency selective channel.

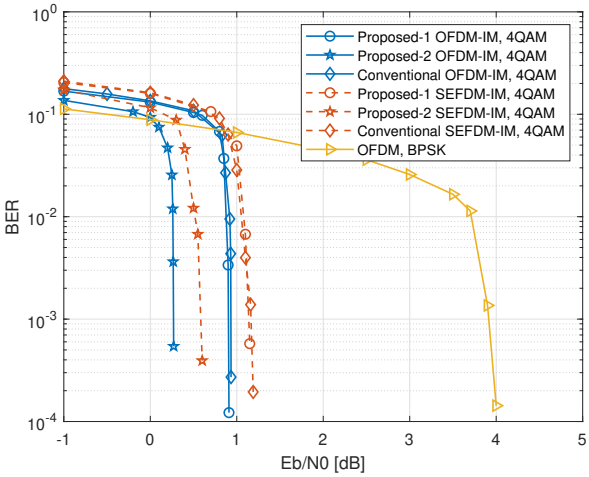

Fig. 5. BER performance of OFDM-IM, SEFDM-IM and OFDM with the spectral efficiency of 0.9 bit/s/Hz in the frequency selective channel.

the proposed-1 design has a much lower D_S value compared to that obtained in the conventional design. The BER performance of SEFDM-IM systems with the three investigated activation designs are degraded due to the inter-subblock ICI, which is caused by non-orthogonally packed subcarriers in different subblocks. Nevertheless, the proposed-2 SEFDM-IM obtains the best BER performance among three SEFDM-IM systems, suggesting that the proposed design principle is robust to ICI impairment. Furthermore, the proposed-2 SEFDM-IM system contaminated by ICI still obtains 0.23 dB and 0.38 dB better performance than the proposed-1 OFDM-IM system and the conventional OFDM-IM system, respectively. It shows that the performance gain brought by the proposed activation pattern design outweighs the performance loss due to ICI. The BER of an OFDM system with BPSK modulation and the coding rate of $R = 0.9$ is also provided. We find that both OFDM-IM and SEFDM-IM systems outperform the OFDM system. Explicitly, the proposed-2 OFDM-IM and the proposed-2 SEFDM-IM systems achieve 3.66 dB and 3.32 dB better BER compared to the OFDM system, respectively.

Figure 3 illustrates the PAPR performance of OFDM-IM, SEFDM-IM and OFDM systems at 0.9 bit/s/Hz. For IM-based systems, their activation patterns have no impact on PAPR. All IM-based systems show substantial performance gain over the traditional OFDM system. More specifically, the OFDM-IM systems achieve 1.85 dB PAPR reduction over their OFDM counterpart at the CCDF of 10^{-2}.

NB-IoT signals only occupy a narrow bandwidth of 180 kHz, and therefore they normally undergo flat fading. Since we consider NB-IoT as the application area of IM-based systems, it is reasonable to adopt the AWGN channel in simulations. To make a fair comparisons of different activation pattern designs in a more challenging channel scenario, a static frequency selective channel described as $h(t) = 0.9137\delta(t)+0.3179\delta(t-2T_s)-0.2532e^{\frac{j\pi}{2}}\delta(t-3T_s)$ is designed, where T_s denotes the sampling period. In Fig. 4, the channel frequency response with a deep frequency notch and two shallow frequency notches is illustrated.

The BER curves in Fig. 5 illustrate that all investigated systems experience performance degradation under the frequency selective channel, compared to the case of AWGN channel in Fig. 2. Nevertheless, the proposed-2 OFDM-IM system maintains its performance advantage over the other two OFDM-IM systems, which shows that the gain of the proposed activation pattern design does not vanish under frequency selective fading. The performance gap between the proposed-1 OFDM-IM and the conventional OFDM-IM becomes negligible. Similar observations are found on the performance of SEFDM-IM systems. Moreover, the proposed-2 SEFDM-IM system still outperforms the proposed-1 OFDM-IM and the conventional OFDM-IM systems. The performance improvement of the proposed-2 OFDM-IM system compared to its OFDM counterpart is decreased by 0.1 dB, indicating that OFDM-IM systems are less robust to frequency selective

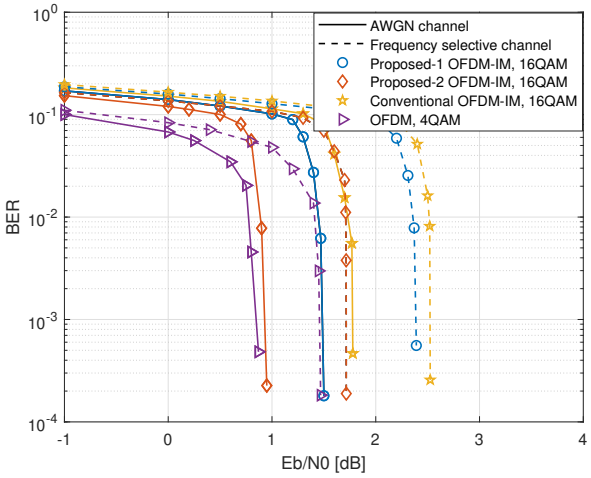

Fig. 6. BER performance of OFDM-IM and OFDM with the spectral efficiency of 1.5 bit/s/Hz in the AWGN channel and the frequency selective channel.

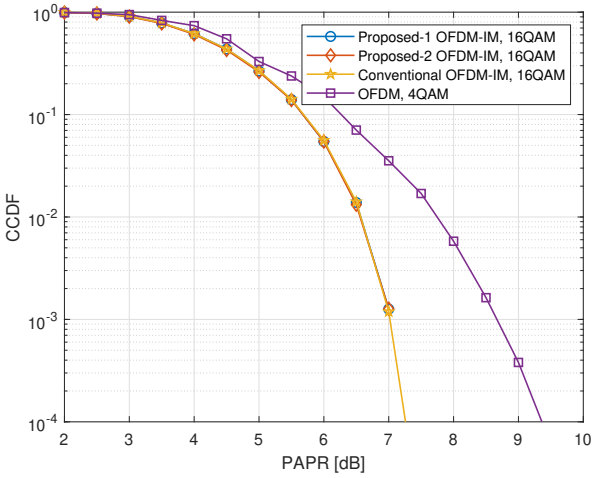

Fig. 7. PAPR distribution of OFDM-IM and OFDM with the spectral efficiency of 1.5 bit/s/Hz.

fading. A subcarrier-level interleaving technique provided in [15] may offer OFDM-IM with improved BER performance.

Although the current 3GPP standard specifies 4QAM as the highest modulation order for NB-IoT, we expect higher-order modulation schemes to be allowed. In Fig. 6, the error performance of three OFDM-IM systems with 16QAM modulation are provided, and their spectral efficiencies are increased to 1.5 bit/s/Hz. SEFDM-IM systems are not considered here as the enhanced bandwidth compression in SEFDM mitigates the requirement for high-order modulation schemes. When the AWGN channel is used, the proposed-2 OFDM-IM obtains 0.83 dB power gain compared to the conventional OFDM-IM system. Furthermore, the error performance of the proposed-2 OFDM-IM system is close to that of the OFDM system with 4QAM modulation and the coding rate of $R = 0.75$. When frequency selective fading is applied, the relative BER performance among the OFDM-IM systems with three activation pattern designs remain unchanged. The performance loss of the proposed-2 OFDM-IM system comparing with the OFDM system slightly increases when experiencing frequency selective fading. Regarding the PAPR performance illustrated in Fig. 7, the three OFDM-IM systems obtain 2 dB better performance than their OFDM counterpart at the 10^{-4} CCDF.

V. Conclusion

In this work, we defined two new parameters namely Hamming distance for similarity and Hamming distance for difference for analytical comparisons of possible activation pattern designs and proposed a min-max Hamming distance design principle. In the coded scenario, the principle was shown effective in improving the BER performance of OFDM-IM and SEFDM-IM systems both with and without frequency selective fading. PAPR distributions of OFDM-IM and SEFDM-IM systems were also presented to illustrate the performance advantage of IM systems over their OFDM counterpart.

References

[1] X. Cheng, M. Zhang, M. Wen, and L. Yang, "Index modulation for 5G: Striving to do more with less," *IEEE Wireless Communications*, vol. 25, no. 2, pp. 126–132, Apr. 2018.

[2] R. Y. Mesleh, H. Haas, S. Sinanovic, C. W. Ahn, and S. Yun, "Spatial modulation," *IEEE Transactions on Vehicular Technology*, vol. 57, no. 4, pp. 2228–2241, 2008.

[3] R. Abu-alhiga and H. Haas, "Subcarrier-index modulation OFDM," in *2009 IEEE 20th International Symposium on Personal, Indoor and Mobile Radio Communications*, 2009, pp. 177–181.

[4] M. Nakao, T. Ishihara, and S. Sugiura, "Single-carrier frequency-domain equalization with index modulation," *IEEE Communications Letters*, vol. 21, no. 2, pp. 298–301, 2017.

[5] T. Mao, Q. Wang, Z. Wang, and S. Chen, "Novel index modulation techniques: A survey," *IEEE Communications Surveys Tutorials*, vol. 21, no. 1, pp. 315–348, 2019.

[6] S. Doğan Tusha, A. Tusha, E. Basar, and H. Arslan, "Multidimensional index modulation for 5G and beyond wireless networks," *Proceedings of the IEEE*, vol. 109, no. 2, pp. 170–199, 2021.

[7] E. Başar, Aygölü, E. Panayırcı, and H. V. Poor, "Orthogonal frequency division multiplexing with index modulation," *IEEE Transactions on Signal Processing*, vol. 61, no. 22, pp. 5536–5549, 2013.

[8] L. Xiao, B. Xu, H. Bai, Y. Xiao, X. Lei, and S. Li, "Performance evaluation in PAPR and ICI for ISIM-OFDM systems," in *2014 International Workshop on High Mobility Wireless Communications*, 2014, pp. 84–88.

[9] T. Mao, Z. Wang, Q. Wang, S. Chen, and L. Hanzo, "Dual-mode index modulation aided OFDM," *IEEE Access*, vol. 5, pp. 50–60, 2017.

[10] T. Xu and I. Darwazeh, "Transmission experiment of bandwidth compressed carrier aggregation in a realistic fading channel," *IEEE Transactions on Vehicular Technology*, vol. 66, no. 5, pp. 4087–4097, May 2017.

[11] Y. Chen, T. Xu, and I. Darwazeh, "Index modulation pattern design for non-orthogonal multicarrier signal waveforms," *IEEE Transactions on Wireless Communications*, 2022.

[12] J. Li, M. Wen, X. Cheng, Y. Yan, S. Song, and M. H. Lee, "Differential spatial modulation with gray coded antenna activation order," *IEEE Communications Letters*, vol. 20, no. 6, pp. 1100–1103, 2016.

[13] X. Li, H. Wang, N. Guan, and W. Lai, "A dual-mode index modulation scheme with gray-coded pairwise index mapping," *IEEE Communications Letters*, vol. 22, no. 8, pp. 1580–1583, 2018.

[14] S. Isam and I. Darwazeh, "Simple DSP-IDFT techniques for generating spectrally efficient FDM signals," in *2010 7th International Symposium on Communication Systems, Networks Digital Signal Processing (CSNDSP 2010)*, 2010, pp. 20–24.

[15] Y. Xiao, S. Wang, L. Dan, X. Lei, P. Yang, and W. Xiang, "OFDM with interleaved subcarrier-index modulation," *IEEE Communications Letters*, vol. 18, no. 8, pp. 1447–1450, 2014.